Three-dimensional magnetic field of a superconducting iron-free quadrupole; application to the CESR Phase III IR quadrupoles

G. Dugan
Cornell University

1. Introduction

The required quality of the magnetic field in the superconducting magnets planned for the CESR Phase III IR region is relatively demanding (integrated harmonics <5 units). Since the magnets are "short" (650 mm effective length) but large in aperture (approximately 100 mm radius), we can expect significant end effects. Hence it will be important to understand and control well the sources of errors in the ends. Moreover, the ends are also the location in which the peak field may occur, which can determine the ultimate quench limit of the magnet. Thus, a calculation of the full three-dimensional magnetic field of the magnets (including realistic ends) will be quite useful in the design stage. A complete evaluation of the field will also be useful in determining its effects on nearby objects in the relatively congested IR area. Since the magnets are iron-free, the field may be determined directly from the current distribution.

The approach to be taken to determine the magnetic field is the following. We want to know the harmonic structure of the field near the quadrupole axis for purposes of beam dynamics, so we would like to do the calculation in a form which leads easily to a harmonic expansion. However, we also want to know the value of the field at its maximum (within the coil), to estimate the quench performance of the magnet. This will require considering a coil package with a finite thickness in the radial direction. The field within the coil cannot be obtained easily from a harmonic expansion.

For these reasons, we take two different approaches to calculating the magnetic field. We start with a current distribution confined to a sheet, described in part 2 below. To obtain a general expression for the field everywhere for a current sheet, we proceed as described in part 3 , and perform a direct integration over the current density to get the vector potential, and then the field. To obtain a harmonic expansion for the current sheet, we use an expansion in cylindrical harmonics for 1/r in the vector potential integral, and obtain harmonic expansions for the potential and field, as described in part 4 below. Then, in part 5, we integrate the results of part 3 over a distribution of current sheets to obtain an expression for the field from a finite thickness coil package. Finally, in part 6, we consider the superposition of several coil blocks, each of the general form shown below, which begins to approximate the situation for a realistic magnet. In part 7, we apply these results to a specific coil configuration which is an example design for the Q1/Q2 CESR Phase III IR magnet.

2. Current Distribution

The basic model for a single coil sheet (one-quarter of the quadrupole) is shown in figure 1.

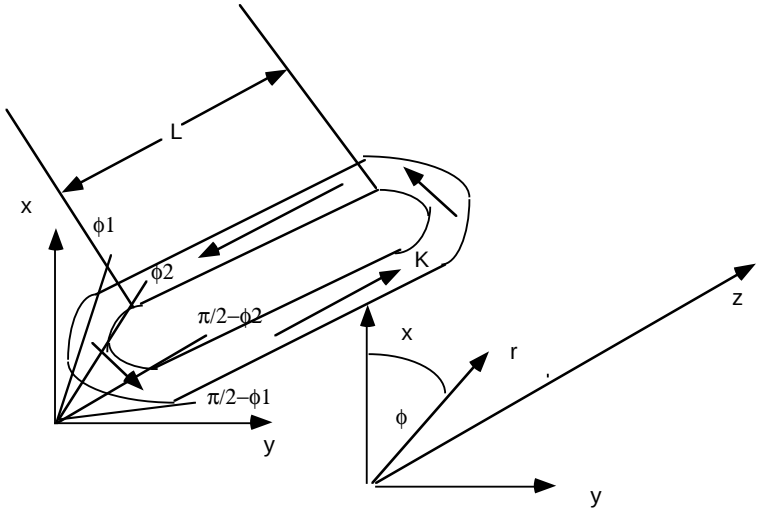

Figure 1

As an approximation to a flat array of wires, the current is taken to flow as a continuous surface current sheet which is divided into 4 regions. One region carries current purely in the z-direction, and extends from z=0 to z=L. In this region, the sheet is curved to conform to a surface of constant cylindrical radius ρ=R, and extends from $\phi=\pi/2-\phi_2$ to $\pi/2-\phi_1$. The current returns symmetrically in another similar region extending from $\phi=\phi_1$ to ϕ_2 (the shell angle of the coil is $\phi_s=\phi_2-\phi_1$). The current densities in these sheets are

$$\vec{K} = \pm\hat{k}\frac{I}{R\phi_s}$$

The regions of the current sheet at the ends are more complicated. Fig 2 shows a detail of the (far: Z>L) end region. In fig 3a and 3b, the coil geometry is laid out in (ζ,θ) coordinates, with the coil, which follows the surface of the cylinder of radius ρ=R, laid out flat.

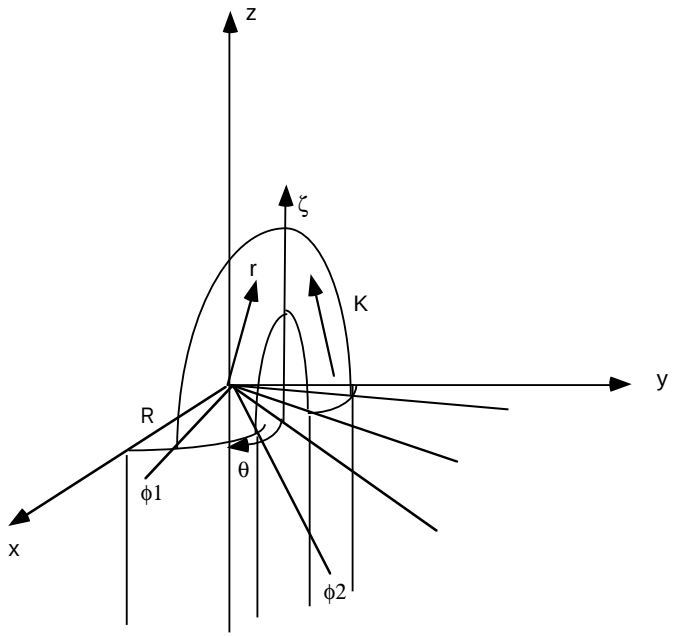

Fig. 2: Coil end geometry (far end)

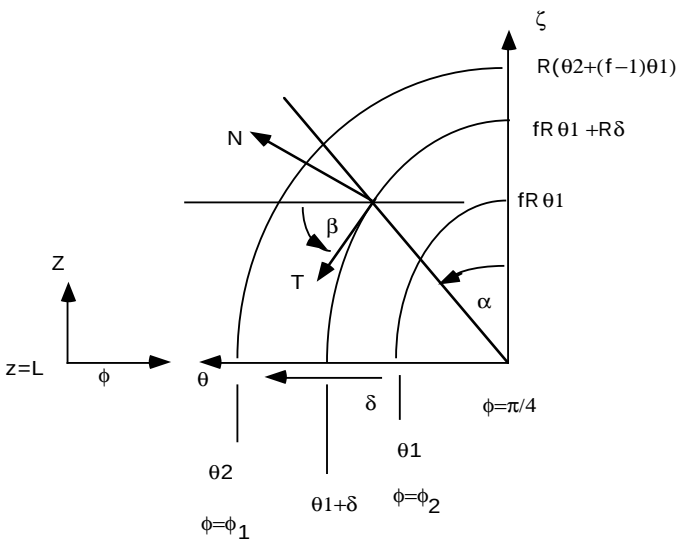

Fig. 3(a)-Far end-left side

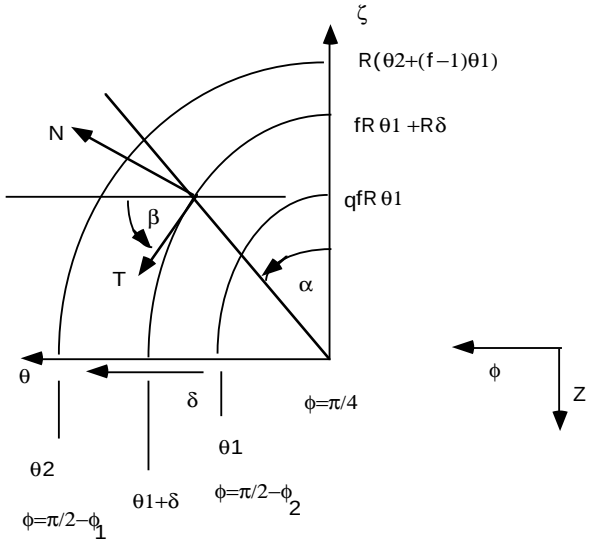

Fig. 3(b)-Near end-right side

In the (ζ-θ) surface, the layout of the coils is described in general by an elliptical relation between ζ and θ:

$$\frac{\theta^2}{(\theta_1+\delta)^2}+\frac{\zeta^2}{R^2(f\theta_1+\delta)^2}=1$$

in which the parameter δ varies from 0 (corresponding to the inner edge of the coils) to $\delta=\phi_s$ (shell angle, corresponding to the outer edge of the coils). This model has a "constant width" coil: the coil width is maintained constant in the (ζ-θ) surface, and δ varies from 0 to ϕ_s , for all α. The aspect ratio of the ellipse will vary with δ. The model can be adapted to a non-constant width coil, by allowing the range of variation of δ to vary with α from 0 to $\delta_{max}(\alpha)$. In this case, we replace ϕ_s with $\delta_{max}(\alpha)$ .The choice f=1 corresponds to a "circular" end. In terms of the ellipse parametric angle α, we have

$$\zeta = R(f\theta_1+\delta)\mathrm{Cos}[\alpha]$$
$$\theta = (\theta_1+\delta)\mathrm{Sin}[\alpha]$$

For the "far" end of the coil (z>L: fig. 3(a)), the relation between (ζ-θ) and (z,ϕ) is

$$\zeta = z-L,\quad z = L+(f\theta_1+\delta)R\mathrm{Cos}(\alpha)$$
$$\theta=\frac{\pi}{4}-\phi,\ \phi=\frac{\pi}{4}-(\theta_1+\delta)\mathrm{Sin}(\alpha)$$

For the "near" end (z<0), the relation is

$$\zeta=-z,\ z=-(f\theta_1+\delta)R\mathrm{Cos}(\alpha)$$
$$\theta=\phi-\frac{\pi}{4},\ \phi=\frac{\pi}{4}+(\theta_1+\delta)\mathrm{Sin}(\alpha)$$

In both cases, $\theta_1=\frac{\pi}{4}-\phi_2$. The current density is assumed to be due to an array of wires which lie along lines of constant δ The current density flows along the direction of the vector T shown in figs 3(a) and 3(b). A current density of this form, which satisfies the requirement of current conservation ($\vec{\nabla}\bullet\vec{K}=0$) is shown in Appendix 4 to be given by

$$\vec{K}(\alpha,\delta) = \frac{I}{R\phi_s}\frac{1}{Cos[\alpha](1+r[\delta]Tan^2[\alpha])}\{\hat{\theta} - \hat{\zeta}r[\delta]Tan[\alpha]\}$$

in which

$$r[\delta] = \frac{f\theta_1 + \delta}{\theta_1 + \delta}$$

For one complete end of a coil (one-quarter of the quadrupole end), the variable α runs from $\pi/2$ to $-\pi/2$, and δ varies from 0 to ϕ_s. At the "far end", the region of $0<\alpha<\pi/2$ corresponds to $0<\phi<\pi/4$, and we have $\hat{\theta} = -\hat{\phi}$, $\hat{\zeta} = \hat{k}$. At the "near" end, $\vec{K}$ changes sign since $\hat{\theta} = \hat{\phi}$, $\hat{\zeta} = -\hat{k}$, and the region $-\pi/2<\alpha<0$ corresponds to $0<\phi<\pi/4$. Note that although the above form for the current density has zero divergence, as required from current conservation, but it does not have zero curl. This is because the model requires the current density to flow in the direction of the wires, which would correspond to a conducting sheet with a conductivity which varies over its surface.

3. Magnetic field of a current sheet by direct integration

The vector potential at a general field point $\vec{r}=(\rho,\phi,z)$, is

$$\vec{A}(\vec{r}) = \frac{\mu_0}{4\pi}\int\frac{\vec{K}(\vec{r}')da}{|\vec{r}-\vec{r}'|}$$

in which

$$\vec{r} = \rho\hat{\rho} + z\hat{k}$$
$$\vec{r}' = \rho'\hat{\rho}' + z'\hat{k}$$

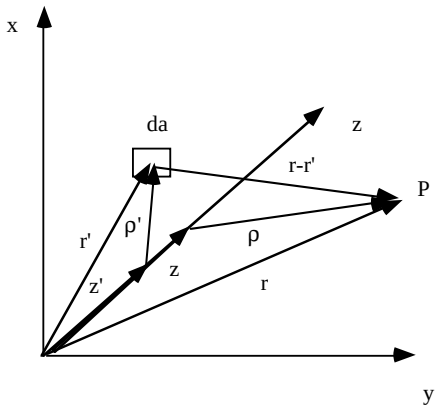

Expanding gives

$$\vec{r} - \vec{r}' = \rho\hat{\rho} - \rho'\hat{\rho}' + (z-z')\hat{k}$$

$$(\vec{r}-\vec{r}')^2 = (\rho\hat{\rho} - \rho'\hat{\rho}')\bullet(\rho\hat{\rho} - \rho'\hat{\rho}') + (z-z')^2$$
$$= \rho^2 + \rho'^2 - 2\rho\rho'\hat{\rho}'\bullet\hat{\rho} + (z-z')^2$$
$$= \rho^2 + \rho'^2 - 2\rho\rho' Cos(\phi-\phi') + (z-z')^2$$

$$\vec{A}(\vec{r}) = \frac{\mu_0 R}{4\pi}\int\frac{dz'd\phi'\vec{K}(\phi',z')}{\sqrt{\rho^2 + R^2 - 2\rho R Cos(\phi-\phi') + (z-z')^2}}$$

The vector potential exhibits the following symmetries, which come from the symmetry of the quadrupole current $\vec{K}$:

$$A_z(\rho,\frac{\pi}{2}-\phi,z)=-A_z(\rho,\phi,z)$$

$$A_\rho(\rho,\frac{\pi}{2}-\phi,z)=-A_\rho(\rho,\phi,z)$$

$$A_\phi(\rho,\frac{\pi}{2}-\phi,z)=A_\phi(\rho,\phi,z)$$

The details of the evaluation of the above integral for the vector potential is given in Appendix 1(a). Once the vector potential is determined, the fields are obtained by taking the curl:

$$B_r(\rho,\phi,z)=\frac{1}{\rho}\frac{\partial A_z}{\partial\phi}-\frac{\partial A_\phi}{\partial z}$$

$$B_\phi(\rho,\phi,z)=\frac{\partial A_\rho}{\partial z}-\frac{\partial A_z}{\partial\rho}$$

$$B_z(\rho,\phi,z)=\frac{1}{\rho}\left[\frac{\partial(\rho A_\phi)}{\partial\rho}-\frac{\partial A_\rho}{\partial\phi}\right]$$

Using the vector potential symmetries, the field symmetries are

$$B_\rho(\rho,\frac{\pi}{2}-\phi,z)=B_\rho(\rho,\phi,z)$$

$$B_\phi(\rho,\frac{\pi}{2}-\phi,z)=-B_\phi(\rho,\phi,z)$$

$$B_z(\rho,\frac{\pi}{2}-\phi,z)=B_z(\rho,\phi,z)$$

The details of the evaluation of the fields is given in Appendix 1(b). The fields from the uniform current distributions at 0<z<L are called "body fields"; those from the ends are called "end fields". The end fields from the "far" end (z>L) and the "near" end (z<0) are related:

$$B_{\text{near end},\rho}(\rho,\phi,L-z)=B_{\text{far end},\rho}(\rho,\phi,z)$$

$$B_{\text{near end},\phi}(\rho,\phi,L-z)=B_{\text{far end},\phi}(\rho,\phi,z)$$

$$B_{\text{near end},z}(\rho,\phi,L-z)=-B_{\text{far end},z}(\rho,\phi,z)$$

Hence we will only give expressions for the "near end" fields. We introduce the scaled variables

$$\eta=\frac{\rho}{R}\quad\chi=\frac{z}{R}\quad s=\frac{L}{R}$$

The body fields, from Appendix 1(b), are

$$B_{\text{body},\rho}(\eta,\phi,\chi)=\frac{\mu_0 I}{4\pi R\phi_s}I_{\text{body},\rho}(\eta,\phi,\chi)\quad B_{\text{body},\phi}(\eta,\phi,\chi)=-\frac{\mu_0 I}{4\pi R\phi_s}I_{\text{body},\phi}(\eta,\phi,\chi)$$

The end fields, from Appendix 1(b), are

$$B_{\text{near end},z}(\eta,\phi,\chi)=\frac{\mu_0 I}{4\pi R\phi_s}\left[I_{1,\text{near}}(\eta,\phi,\chi)-\eta\left(\text{Cos}[\phi-\frac{\pi}{4}]I_{2,\text{near}}(\eta,\phi,\chi)-\text{Sin}[\phi-\frac{\pi}{4}]I_{3,\text{near}}(\eta,\phi,\chi)\right)\right]$$

$$B_{\text{near end},\phi}(\eta,\phi,\chi)=\frac{\mu_0 I}{4\pi R\phi_s}\left[-\eta I_{6,\text{near}}(\eta,\phi,\chi)+\text{Cos}[\phi-\frac{\pi}{4}]I_{5,\text{near}}(\eta,\phi,\chi)-\text{Sin}[\phi-\frac{\pi}{4}]I_{4,\text{near}}(\eta,\phi,\chi)\right]$$

$$B_{\text{near end},\rho}(\eta,\phi,\chi) = \frac{\mu_0 I}{4\pi R\phi_s}\left[\text{Cos}[\phi-\frac{\pi}{4}]I_{4,\text{near}}(\eta,\phi,\chi) + \text{Sin}[\phi-\frac{\pi}{4}]I_{5,\text{near}}(\eta,\phi,\chi)\right]$$

The integrals are derived in Appendix 1(b) and are:

$$I_{\text{body},\rho}(\eta,\phi,\chi) = \frac{\mu_0 I}{4\pi R\phi_s}\int_{\phi_1}^{\phi_2} d\phi' \left(\begin{array}{l} \dfrac{\text{Sin}(\phi-\phi')}{1+\eta^2-2\eta\text{Cos}(\phi-\phi')}\left(\dfrac{\chi}{\sqrt{1+\eta^2+\chi^2-2\eta\text{Cos}(\phi-\phi')}} + \dfrac{s-\chi}{\sqrt{1+\eta^2+(\chi-s)^2-2\eta\text{Cos}(\phi-\phi')}}\right) \\ + \dfrac{\text{Cos}(\phi+\phi')}{1+\eta^2-2\eta\text{Sin}(\phi+\phi')}\left(\dfrac{\chi}{\sqrt{1+\eta^2+\chi^2-2\eta\text{Sin}(\phi+\phi')}} + \dfrac{s-\chi}{\sqrt{1+\eta^2+(\chi-s)^2-2\eta\text{Sin}(\phi+\phi')}}\right) \end{array}\right)$$

$$I_{\text{body},\phi}(\eta,\phi,\chi) = -\frac{\mu_0 I}{4\pi R\phi_s}\int_{\phi_1}^{\phi_2} d\phi' \left(\begin{array}{l} \dfrac{\eta-\text{Cos}(\phi-\phi')}{1+\eta^2-2\eta\text{Cos}(\phi-\phi')}\left(\dfrac{\chi}{\sqrt{1+\eta^2+\chi^2-2\eta\text{Cos}(\phi-\phi')}} + \dfrac{s-\chi}{\sqrt{1+\eta^2+(\chi-s)^2-2\eta\text{Cos}(\phi-\phi')}}\right) \\ - \dfrac{\eta-\text{Sin}(\phi+\phi')}{1+\eta^2-2\eta\text{Sin}(\phi+\phi')}\left(\dfrac{\chi}{\sqrt{1+\eta^2+\chi^2-2\eta\text{Sin}(\phi+\phi')}} + \dfrac{s-\chi}{\sqrt{1+\eta^2+(\chi-s)^2-2\eta\text{Sin}(\phi+\phi')}}\right) \end{array}\right)$$

$$I_{1,\text{near}}(\eta,\phi,\chi) = \int_0^{\phi_s}(\theta_1+\delta)d\delta\int_0^{\frac{\pi}{2}} d\alpha\left(g'_{\text{near}+}(\eta,\phi,\chi,\delta,\alpha) + g'_{\text{near}-}(\eta,\phi,\chi,\delta,\alpha)\right)$$

$$I_{2,\text{near}}(\eta,\phi,\chi) = \int_0^{\phi_s}(\theta_1+\delta)d\delta\int_0^{\frac{\pi}{2}} d\alpha\text{Cos}(h(\alpha,\delta))\text{Cos}[\alpha]\left(g'_{\text{near}+}(\eta,\phi,\chi,\delta,\alpha) + g'_{\text{near}-}(\eta,\phi,\chi,\delta,\alpha)\right)$$

$$I_{3,\text{near}}(\eta,\phi,\chi) = \int_0^{\phi_s}(\theta_1+\delta)d\delta\int_0^{\frac{\pi}{2}} d\alpha\text{Sin}(h(\alpha,\delta))\text{Cos}[\alpha]\left(g'_{\text{near}+}(\eta,\phi,\chi,\delta,\alpha) - g'_{\text{near}-}(\eta,\phi,\chi,\delta,\alpha)\right)$$

$$I_{4,\text{near}}(\eta,\phi,\chi) = \int_0^{\phi_s} d\delta\int_0^{\frac{\pi}{2}} d\alpha\text{Cos}[\alpha]\left[(f\theta_1+\delta)\text{Sin}(h(\alpha,\delta))\text{Tan}[\alpha] + (\theta_1+\delta)(\chi+(f\theta_1+\delta)\text{Cos}[\alpha])\text{Cos}(h(\alpha,\delta))\right]\left(g'_{\text{near}+}(\eta,\phi,\chi,\delta,\alpha) + g'_{\text{near}-}(\eta,\phi,\chi,\delta,\alpha)\right)$$

$$I_{5,\text{near}}(\eta,\phi,\chi) = \int_0^{\phi_s} d\delta\int_0^{\frac{\pi}{2}} d\alpha\text{Cos}[\alpha]\left[(f\theta_1+\delta)\text{Cos}(h(\alpha,\delta))\text{Tan}[\alpha] - (\theta_1+\delta)(\chi+(f\theta_1+\delta)\text{Cos}[\alpha])\text{Sin}(h(\alpha,\delta))\right]\left(g'_{\text{near}+}(\eta,\phi,\chi,\delta,\alpha) - g'_{\text{near}-}(\eta,\phi,\chi,\delta,\alpha)\right)$$

in which

$$g'_{\text{near}\pm}(\eta,\phi,\chi,,\delta,\alpha) = \frac{1}{\sqrt{\eta^2+1-2\eta\text{Cos}(\phi-\frac{\pi}{4}\pm h(\alpha,\delta)) + (\chi+(f\theta_1+\delta)\text{Cos}[\alpha])^2}^3}$$

and

$$h(\alpha,\delta) = (\theta_1+\delta)\text{Sin}[\alpha]$$

The integrals depend on the detailed geometry of the coil ends. Note that the above results are only for the fields from one quadrant of the quadrupole.

4. Magnetic field of a current sheet by harmonic expansion

We return to the expression for the vector potential

$$\vec{A}(\vec{r}) = \frac{\mu_0}{4\pi}\int \frac{\vec{K}(\vec{r}')da}{|\vec{r}-\vec{r}'|}$$

and use the following expansion:

$$\frac{1}{|\vec{r}-\vec{r}'|} = \sum_{m=-\infty}^{\infty}\int_0^{\infty} dk Exp[im(\phi-\phi')]Exp[-k(z_> - z_<)]J_m(k\rho)J_m(k\rho')$$

This form is an explicit expansion of 1/r in cylindrical harmonics. One substitutes this into the expression for the vector potential, and the integral over k gives Legendre Q-functions. These may be power-series expanded to obtain a power series for each harmonic of the vector potential. A significant simplification in the harmonic structure results when one adds the potentials from all four quadrants of the quadrupole. The details are given in Appendix 3(a). One then takes the curl to get a series expansion for the field. The symmetries given above for the field require that the most general harmonic expansion have the following form (for a field from a perfectly symmetric arrangement of four quadrupole coils):

$$B_\rho(\rho,\phi,z) = \sum_{k=1,3,5,..}^{\infty} b_{\rho,k}(\rho,z)Sin[2k\phi];\ B_\phi(\rho,\phi,z) = \sum_{k=1,3,5,..}^{\infty} a_{\phi,k}(\rho,z)Cos[2k\phi];\ B_z(\rho,\phi,z) = \sum_{k=1,3,5,..}^{\infty} b_{z,k}(\rho,z)Sin[2k\phi]$$

The results, derived in Appendix 3(b), are the following. The body fields for the complete quadrupole are

$$\vec{B}_{body}(\rho,\phi,z) = G\rho_0 \sum_{k\ odd}\left[\frac{\rho}{\rho_0}\right]^{2k-1}\vec{\vec{V}}_k(\phi)\bullet\sum_{r=0}\left[\frac{\rho}{\rho_0}\right]^r\vec{\delta}^{body}(r,k,\chi)$$

in which the azimuthal dependence is described by the matrix

$$\vec{\vec{V}}_k(\phi) = \begin{Bmatrix} Sin(2k\phi) & 0 & 0 \\ 0 & Cos(2k\phi) & 0 \\ 0 & 0 & Sin(2k\phi) \end{Bmatrix}$$

the field gradient is

$$G = \frac{4\mu_0 I Sin[\phi_s]Cos[2\phi_1+\phi_s]}{\pi\phi_s R^2}$$

and ρ_0 is the reference radius. The components of the harmonic coefficient vector are shown in Appendix 3(b) to be

$$\delta_\phi^{body}(r,k,\chi) = \left[\frac{\rho_0}{R}\right]^{2k-2+2r}\frac{2(k+r)(-1)^r Sin[k\phi_s]Cos[k(2\phi_1+\phi_s)]}{2^{2k+r}Sin[\phi_s]Cos[2\phi_1+\phi_s]k}\sum_{j=0}^{r}\frac{(4k-1+2r+2j)!!}{(2k+j)!(r-j)!j!2^j}(-1)^j\left[(s-\chi)_2F_1(\frac{1}{2},2k+r+j+\frac{1}{2};\frac{3}{2};-(s-\chi)^2)+\chi_2F_1(\frac{1}{2},2k+r+j+\frac{1}{2};\frac{3}{2};-\chi^2)\right]$$

$$\delta_\rho^{body}(r,k,\chi) = \left[\frac{\rho_0}{R}\right]^{2k-2+2r}\frac{2(-1)^r Sin[k\phi_s]Cos[k(2\phi_1+\phi_s)]}{2^{2k+r}Sin[\phi_s]Cos[2\phi_1+\phi_s]}\sum_{j=0}^{r}\frac{(4k-1+2r+2j)!!}{(2k+j)!(r-j)!j!2^j}(-1)^j\left[(s-\chi)_2F_1(\frac{1}{2},2k+r+j+\frac{1}{2};\frac{3}{2};-(s-\chi)^2)+\chi_2F_1(\frac{1}{2},2k+r+j+\frac{1}{2};\frac{3}{2};-\chi^2)\right]$$

$$\delta_z^{body}(r,k,\chi) = 0$$

in which ${}_2F_1$ is a hypergeometric function.

For the ends, we have

$$\vec{B}_{ends}(\rho,\phi,z) = G\rho_0 \sum_{k\ odd}\left[\frac{\rho}{\rho_0}\right]^{2k-1}\vec{\vec{V}}_k(\phi)\bullet\sum_{r=0}\left[\frac{\rho}{\rho_0}\right]^{2r}\vec{\delta}^{ends}(r,k,\chi)$$

in which the components of the harmonic coefficient vector are

$$\delta_\rho^{near\ end}(r,k,\chi) = \frac{(-1)^{\frac{k-1}{2}+r}}{2^{2k+r+1}Sin[\phi_s]Cos[2\phi_1+\phi_s]}\left[\frac{\rho_0}{R}\right]^{2k-2+2r}\sum_{j=0}^{r}\delta'^{near\ end}_\rho(j,r,k,\chi)$$

$$\delta_{\rho}'^{\text{near end}}(j,r,k,\chi)=\frac{(4k-1+2r+2j)!!}{(2k+j)!(r-j)!\,j!2^{j}}(-1)^{j}\int_{0}^{\phi_s}d\delta\int_{0}^{\frac{\pi}{2}}d\alpha\,\text{Cos}[2kh(\alpha,\delta)]\text{Cos}[\alpha]\left[\sqrt{\frac{1}{1+\left(\chi+(f\theta_1+\delta)\text{Cos}[\alpha]\right)^2}}\right]^{4k+2r+2j+1}$$

$$\left[4k(f\theta_1+\delta)\text{Tan}[\alpha]\text{Tan}[2kh(\alpha,\delta)]+2(\theta_1+\delta)\left(\chi+(f\theta_1+\delta)\text{Cos}[\alpha]\right)\left[2k+j-\frac{(4k+1+2r+2j)(r-j)}{2(2k+j+1)}\frac{1}{1+\left(\chi+(f\theta_1+\delta)\text{Cos}[\alpha]\right)^2}\right]\right]$$

$$\delta_{\phi}^{\text{near end}}(r,k,\chi)=\frac{(-1)^{\frac{k-1}{2}+r}}{2^{2k+r+1}\text{Sin}[\phi_s]\text{Cos}[2\phi_1+\phi_s]}\left[\frac{\rho_0}{R}\right]^{2k-2+2r}\sum_{j=0}^{r}\delta_{\phi}'^{\text{near end}}(j,r,k,\chi)$$

$$\delta_{\phi}'^{\text{near end}}(j,r,k,\chi)=\frac{(4k-1+2r+2j)!!}{(2k+j)!(r-j)!\,j!2^{j}}(-1)^{j}\int_{0}^{\phi_s}d\delta\int_{0}^{\frac{\pi}{2}}d\alpha\,\text{Cos}[2kh(\alpha,\delta)]\text{Cos}[\alpha]\left[\sqrt{\frac{1}{1+\left(\chi+(f\theta_1+\delta)\text{Cos}[\alpha]\right)^2}}\right]^{4k+2r+2j+1}$$

$$\left[(4k+4r)(f\theta_1+\delta)\text{Tan}[\alpha]\text{Tan}[2kh(\alpha,\delta)]+2(\theta_1+\delta)\left(\chi+(f\theta_1+\delta)\text{Cos}[\alpha]\right)\left[2k+j+\frac{(4k+1+2r+2j)(r-j)}{2(2k+j+1)}\frac{1}{1+\left(\chi+(f\theta_1+\delta)\text{Cos}[\alpha]\right)^2}\right]\right]$$

$$\delta_{z}^{\text{near end}}(r,k,\chi)=\frac{(-1)^{\frac{k-1}{2}+r}}{2^{2k+r+1}\text{Sin}[\phi_s]\text{Cos}[2\phi_1+\phi_s]}\left[\frac{\rho_0}{R}\right]^{2k-3+2r}\sum_{j=1}^{r}\delta_{z}'^{\text{near end}}(j,r,k,\chi)$$

$$\delta_{z}'^{\text{near end}}(j,r,k,\chi)=\frac{(4k-1+2r+2j)!!}{(2k+j)!(r-j)!\,j!2^{j}}(-1)^{j}\int_{0}^{\phi_s}d\delta(\theta_1+\delta)\int_{0}^{\frac{\pi}{2}}d\alpha\,\text{Cos}[2kh(\alpha,\delta)]\text{Cos}[\alpha]$$

$$\left[\sqrt{\frac{1}{1+\left(\chi+(f\theta_1+\delta)\text{Cos}[\alpha]\right)^2}}\right]^{4k+2r+2j-1}\left[\frac{4r(2k+j)}{(4k+2r+2j-1)}-\frac{2(r-j)(2k+r)}{(2k+j+1)}\frac{1}{(1+\left(\chi+(f\theta_1+\delta)\text{Cos}[\alpha]\right)^2)}\right]$$

The above results give the full dependence of the field on ρ,ϕ, and z; however, often we are only interested in the harmonics of the integrated field. Expressions are given in Appendix 3(b) for integrals of the harmonics over a limited region of the magnet. For the integrals over the whole magnet, we have

$$\vec{B}_{\text{body}}^{\text{int}}(\rho,\phi)=\int_{-\infty}^{\infty}dz\vec{B}_{\text{body}}(\rho,\phi,z)=RG\rho_0\sum_{k\ \text{odd}}\left[\frac{\rho}{\rho_0}\right]^{2k-1}\vec{\bar{V}}_k(\phi)\bullet\sum_{r=0}\left[\frac{\rho}{\rho_0}\right]^{2r}\vec{\bar{\delta}}^{\text{body,tot}}(r,k)$$

$$\vec{B}_{\text{ends}}^{\text{int}}(\rho,\phi)=\int_{-\infty}^{\infty}dz\vec{B}_{\text{end}}(\rho,\phi,z)=RG\rho_0\sum_{k\ \text{odd}}\left[\frac{\rho}{\rho_0}\right]^{2k-1}\vec{\bar{V}}_k(\phi)\bullet\sum_{r=0}\left[\frac{\rho}{\rho_0}\right]^{2r}(\vec{\bar{\delta}}^{\text{far end,tot}}(r,k)+\vec{\bar{\delta}}^{\text{near end,tot}}(r,k))$$

$$\vec{B}_{\text{total}}^{\text{int}}(\rho,\phi)=\vec{B}_{\text{body}}^{\text{int}}(\rho,\phi)+\vec{B}_{\text{ends}}^{\text{int}}(\rho,\phi)$$

in which the integrated harmonics, from Appendix 3(b), are

$$\bar{\delta}_{\phi}^{\text{body,tot}}(r,k)=\delta_{r,0}s\left[\frac{\rho_0}{R}\right]^{2k-2}\frac{\text{Sin}[k\phi_s]\text{Cos}[k(2\phi_1+\phi_s)]}{\text{Sin}[\phi_s]\text{Cos}[2\phi_1+\phi_s]k}=\bar{\delta}_{\rho}^{\text{body,tot}}(r,k)$$

$$\bar{\delta}_{\phi}^{\text{near end,tot}}(r,k)=\delta_{r,0}\frac{(-1)^{\frac{k-1}{2}}}{\text{Sin}[\phi_s]\text{Cos}[2\phi_1+\phi_s]}\left[\frac{\rho_0}{R}\right]^{2k-2}\int_{0}^{\phi_s}d\delta(f\theta_1+\delta)\int_{0}^{\frac{\pi}{2}}d\alpha\,\text{Sin}[2kh(\alpha,\delta)]\text{Sin}[\alpha]=\bar{\delta}_{\rho}^{\text{near end,tot}}(r,k)$$

$$\bar{\delta}_z^{\text{near end,tot}}(r,k) = \delta_{r,1}\frac{(-1)^{\frac{k-1}{2}}}{\text{Sin}[\phi_s]\text{Cos}[2\phi_1+\phi_s]}\left[\frac{\rho_0}{R}\right]^{2k-1}\int_0^{\phi_s} d\delta(\theta_1+\delta)\int_0^{\frac{\pi}{2}} d\alpha \text{Cos}[2kh(\alpha,\delta)]\text{Cos}[\alpha]$$

Note that since

$$\delta_{\rho,\phi}^{\text{near end}}(r,k,\chi) = \delta_{\rho,\phi}^{\text{far end}}(r,k,s-\chi)\ ;\delta_z^{\text{near end}}(r,k,\chi) = -\delta_z^{\text{far end}}(r,k,s-\chi)$$

the integrated harmonics for the ρ and ϕ components from the two ends add, but cancel for the z component. The z-component may still be important if the beam optics are such that the beam couples to it differently at the two ends of the magnet.

The standard 2D representation of the integrated field in terms of error harmonics is

$$B_\rho^{\text{int}}(\rho,\phi) = B_0 L_{\text{eff}}\sum_n\left[\frac{\rho}{\rho_0}\right]^{n-1}\left(b_n\text{Sin}[n\phi]-a_n\text{Cos}[n\phi]\right)$$

$$B_\phi^{\text{int}}(\rho,\phi) = B_0 L_{\text{eff}}\sum_n\left[\frac{\rho}{\rho_0}\right]^{n-1}\left(b_n\text{Cos}[n\phi]+a_n\text{Sin}[n\phi]\right)$$

where B_0 is the reference field (=$G\rho_0$ for a quadrupole). Hence the correspondence with the harmonics defined in this report becomes

$$L_{\text{eff}} b_{2k} = R[\bar{\delta}_\rho^{\text{far end,tot}}(0,k)+\bar{\delta}_\rho^{\text{near end,tot}}(0,k)+\bar{\delta}_\rho^{\text{body,tot}}(0,k)]$$

Explicitly, including both ends,

$$s_{\text{eff}} b_{2k} = \left[\frac{\rho_0}{R}\right]^{2k-2}\frac{s\text{Sin}[k\phi_s]\text{Cos}[k(2\phi_1+\phi_s)]}{\text{Sin}[\phi_s]\text{Cos}[2\phi_1+\phi_s]k}+2\frac{(-1)^{\frac{k-1}{2}}}{\text{Sin}[\phi_s]\text{Cos}[2\phi_1+\phi_s]}\left[\frac{\rho_0}{R}\right]^{2k-2}\bar{I}(k)$$

$$b_{2k} = \left[\frac{\rho_0}{R}\right]^{2k-2}\frac{s}{s_{\text{eff}}\text{Sin}[\phi_s]\text{Cos}[2\phi_1+\phi_s]}\left[\frac{\text{Sin}[k\phi_s]\text{Cos}[k(2\phi_1+\phi_s)]}{k}+\frac{2(-1)^{\frac{k-1}{2}}}{s}\bar{I}(k)\right]$$

in which

$$\bar{I}(k) = \int_0^{\phi_s} d\delta(f\theta_1+\delta)\int_0^{\frac{\pi}{2}} d\alpha \text{Sin}[2kh(\alpha,\delta)]\text{Sin}[\alpha]$$

Using

$$2\text{Sin}[k\phi_s]\text{Cos}[k(2\phi_1+\phi_s)] = 2\text{Sin}[k(\phi_2-\phi_1)]\text{Cos}[k(\phi_2+\phi_1)] = \text{Sin}[2k\phi_2]-\text{Sin}[2k\phi_1]$$

this becomes

$$b_{2k} = \left[\frac{\rho_0}{R}\right]^{2k-2}\frac{s}{s_{\text{eff}}\text{Sin}[\phi_s]\text{Cos}[2\phi_1+\phi_s]}\left[\frac{\text{Sin}[2k\phi_2]-\text{Sin}[2k\phi_1]}{2k}+\frac{2(-1)^{\frac{k-1}{2}}}{s}\bar{I}(k)\right]$$

For a single coil shell with $\phi_2=\phi_s$, $\phi_1=0$, we get

$$b_{2k} = \left[\frac{\rho_0}{R}\right]^{2k-2}\frac{s\text{Sin}[2k\phi_s]}{s_{\text{eff}}k\text{Sin}[2\phi_s]}\left[1+\frac{4k(-1)^{\frac{k-1}{2}}}{s\text{Sin}[2k\phi_s]}\bar{I}(k)\right]$$

The effective length is determined by requiring that $b_2 = 1$:

$$1 = \frac{s}{s_{eff}}\left[1 + \frac{4}{sSin[2\phi_s]}\bar{I}(1)\right], \quad L_{eff} = L\left[1 + \frac{4}{sSin[2\phi_s]}\bar{I}(1)\right]$$

Then

$$b_{2k} = \left[\frac{\rho_0}{R}\right]^{2k-2} \frac{Sin[2k\phi_s]}{kSin[2\phi_s]} \frac{\left[1 + \frac{4k(-1)^{\frac{k-1}{2}}}{sSin[2k\phi_s]}\bar{I}(k)\right]}{\left[1 + \frac{4}{sSin[2\phi_s]}\bar{I}(1)\right]}$$

In terms of the simple 2D harmonic,

$$b_{2k}(2D) = \left[\frac{\rho_0}{R}\right]^{2k-2} \frac{Sin[2k\phi_s]}{kSin[2\phi_s]}$$

we have

$$b_{2k} = b_{2k}(2D) \frac{\left[1 + \frac{4k(-1)^{\frac{k-1}{2}}}{sSin[2k\phi_s]}\bar{I}(k)\right]}{\left[1 + \frac{4}{sSin[2\phi_s]}\bar{I}(1)\right]}$$

The first term is due only to the body ; the second term is due to the ends and scales like 1/s=R/L. The longitudinal field at the ends can also be written in terms of an "integrated harmonic"

$$B_z^{int}(\rho,\phi) = B_0 L_{eff} \sum_n \left[\frac{\rho}{\rho_0}\right]^n \hat{b}_n Sin[n\phi]$$

except that the integral is only over one end of the magnet (since the contributions from both ends cancel). Note that the (n=2) (quadrupole) harmonic varies as ρ^2 . Then

$$L_{eff}\hat{b}_{2k} = R[\bar{\delta}_z^{near\ end,tot}(1,k)]$$

$$\hat{b}_{2k} = \frac{(-1)^{\frac{k-1}{2}}}{s_{eff}Sin[\phi_s]Cos[2\phi_1 + \phi_s]}\left[\frac{\rho_0}{R}\right]^{2k-1} \int_0^{\phi_s} d\delta(\theta_1 + \delta) \int_0^{\frac{\pi}{2}} d\alpha Cos[2kh(\alpha,\delta)]Cos[\alpha]$$

$$= \frac{(-1)^{\frac{k-1}{2}}}{s_{eff}Sin[\phi_s]Cos[2\phi_1 + \phi_s]}\left[\frac{\rho_0}{R}\right]^{2k-1} \bar{I}_z(k)$$

in which

$$\bar{I}_z(k) = \int_0^{\phi_s} d\delta(\theta_1 + \delta) \int_0^{\frac{\pi}{2}} d\alpha Cos[2kh(\alpha,\delta)]Cos[\alpha]$$

5. Magnetic field of a quadrupole current block

The results given in section 3 above are for the fields from the current sheet described in section 2. As noted in the introduction, for an estimate of the peak field in the magnet's coil, one must of course calculate for a finite thickness coil block. In general, the approach is to use the results of section 3 for B as a function of the sheet radius R, and then integrate over a range of R from R_1 to R_2:

$$d\vec{B} = \frac{I}{R_2 - R_1}\vec{f}(R)dR, \quad \tilde{\vec{B}} = \int dB = \frac{I}{R_2 - R_1}\int_{R_1}^{R_2} \vec{f}(R)dR$$

in which $\vec{f}(R) = \frac{\vec{B}}{I}$, with $\vec{B}$ from section 3 above. Over the R range from R_1 to R_2, we take the current in each infinitesimal shell of thickness dR to be constant:

$$dI = \frac{I}{R_2 - R_1} dR$$

which means that the volume current density, J=dI/(RdRdϕ), decreases as 1/R. This will be the case if the same number of turns are wound in each radial layer, as is the case for magnets wound with keystoned Rutherford cable. The cross-sectional geometry , and a graph of the "near end" R-z geometry, is shown in fig. 4.

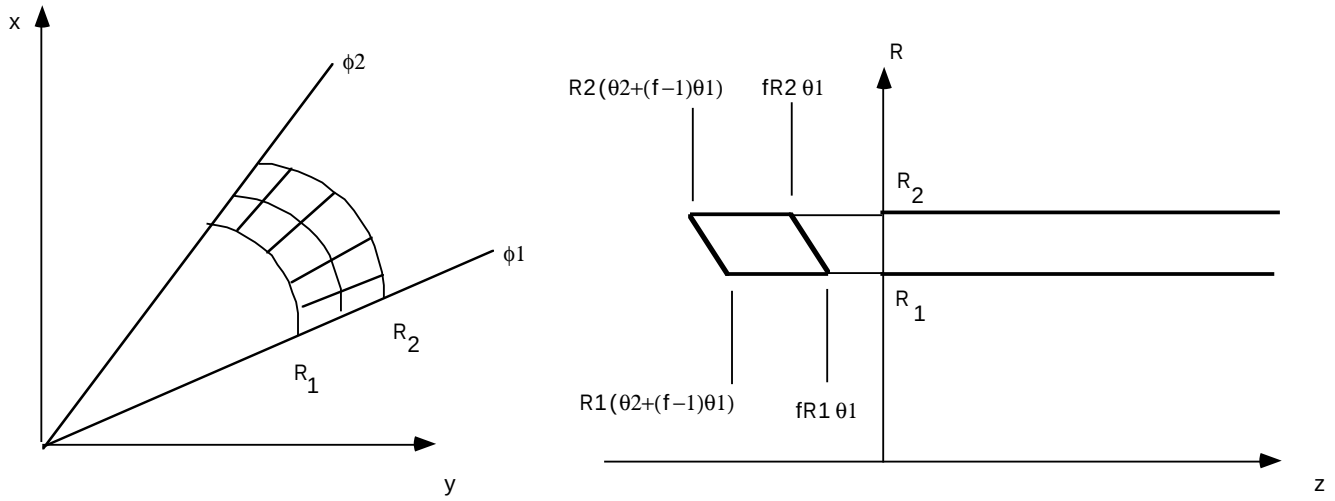

Fig. 4

The integral over R can be done analytically. The details of the calculation are given in Appendix 2. There are some complications due to the fact that the integrands of the final integrals over α and δ (which must be done numerically) are singular when the field point is within the coil block. The integrals giving the fields are, of course, finite, but when doing these integrals numerically (see below, section 7), care must be used in the vicinity of the singular point. The strategy for dealing with this problem is given in Appendix 2. The general form of the results are

$$\tilde{B}_{body,\rho}(\rho,\phi,z) = \frac{\mu_0 I}{4\pi\phi_s(R_2 - R_1)} \tilde{I}_{body,\rho}(\rho,\phi,z)$$

$$\tilde{B}_{body,\phi}(\rho,\phi,z) = -\frac{\mu_0 I}{4\pi\phi_s(R_2 - R_1)} \tilde{I}_{body,\phi}(\rho,\phi,z)$$

$$\tilde{B}_{near\ end,z}(\vec{r}) = \frac{\mu_0 I}{4\pi\phi_s(R_2 - R_1)}\left[\tilde{I}_{1,near}(\rho,\phi,z) - \rho\left(\mathrm{Cos}[\phi - \frac{\pi}{4}]\tilde{I}_{2,near}(\rho,\phi,z) - \mathrm{Sin}[\phi - \frac{\pi}{4}]\tilde{I}_{3,near}(\rho,\phi,z)\right)\right]$$

$$\tilde{B}_{near\ end,\phi}(\vec{r}) = \frac{\mu_0 I}{4\pi\phi_s(R_2 - R_1)}\left[-\rho\tilde{I}_{6,near}(\rho,\phi,z) + \mathrm{Cos}[\phi - \frac{\pi}{4}]\tilde{I}_{5,near}(\rho,\phi,z) - \mathrm{Sin}[\phi - \frac{\pi}{4}]\tilde{I}_{4,near}(\rho,\phi,z)\right]$$

$$\tilde{B}_{near\ end,\rho}(\vec{r}) = \frac{\mu_0 I}{4\pi\phi_s(R_2 - R_1)}\left[\mathrm{Cos}[\phi - \frac{\pi}{4}]\tilde{I}_{4,near}(\rho,\phi,z) + \mathrm{Sin}[\phi - \frac{\pi}{4}]\tilde{I}_{5,near}(\rho,\phi,z)\right]$$

The integrals $\tilde{I}$ in the above equations are similar to those quoted in section 3, and are given in Appendix 2. This is still just for one-quarter of the quadrupole. We must sum over the other three quadrants to get the total quadrupole field:

$$\vec{B}_{body}(\vec{r}) = \sum_{j=0}^{3}(-1)^j \vec{\tilde{B}}_{body}(\vec{r}, \phi - j\frac{\pi}{2})$$

$$\vec{B}_{near\ \ end}(\vec{r}) = \sum_{j=0}^{3}(-1)^j \vec{\tilde{B}}_{near\ end}(\vec{r}, \phi - j\frac{\pi}{2})$$

The effective gradient is given by

$$\tilde{G} = \int d\tilde{G}$$

$$d\tilde{G} = \frac{4\mu_0 dI Sin[\phi_S] Cos[2\phi_1 + \phi_S]}{\pi \phi_S R^2} = \frac{4\mu_0 I Sin[\phi_S] Cos[2\phi_1 + \phi_S]}{\pi \phi_S (R_2 - R_1)} \frac{dR}{R^2}$$

$$\tilde{G} = \frac{4\mu_0 I Sin[\phi_S] Cos[2\phi_1 + \phi_S]}{\pi \phi_S (R_2 - R_1)} \int_{R_1}^{R_2} \frac{dR}{R^2} = \frac{4\mu_0 I Sin[\phi_S] Cos[2\phi_1 + \phi_S]}{\pi \phi_S (R_2 - R_1)} \frac{(R_2 - R_1)}{R_2 R_1} = \frac{4\mu_0 I Sin[\phi_S] Cos[2\phi_1 + \phi_S]}{\pi \phi_S R_2 R_1}$$

6. Magnetic field of a multiple quadrupole coil

Finally, we consider the superposition of several (N) coils. Two or more coils are used to reduce the peak field in the ends by spreading out the current distribution and lowering the current density. The use of two coils, with appropriate geometry differences, also allows the b_6 end harmonic from one coil to cancel that from the other. Each coil is of the form described above, and has a geometry described by the following parameters (for coil i):

$\phi_1(i)$: initial coil azimuthal angle

$\phi_2(i)$: final coil azimuthal angle

$\phi_s(i)$: coil shell angle=$\phi_2(i)$-$\phi_1(i)$

$\theta_1(i)=\pi/4-\phi_2(i)$

f(i): elliptical parameter for coil i

$\Delta(i)$: z-offset for coil i (straight part of coil starts at z=-$\Delta(i)$ for the near end)

Length of straight part of coil i=$L_0+2\Delta(i)$

I(i): current in coil i

The geometry is shown (for the "near" end) in fig. 5 for N=2

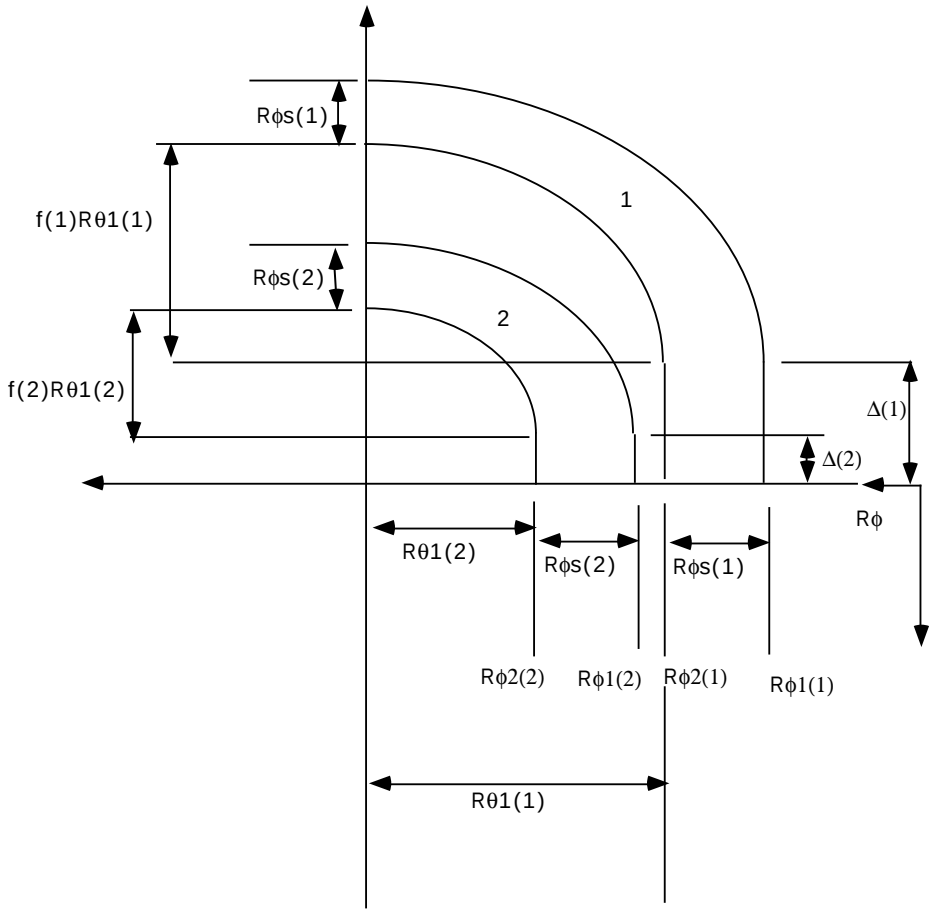

Fig. 5

Then the total field will be of the general form

$$\tilde{\vec{B}}_{tot}(\vec{r}) = \frac{\mu_0}{4\pi(R_2 - R_1)} \sum_{i=1}^{N} \frac{I(i)}{\phi_s(i)} \tilde{I}(\rho, \phi, z + \Delta(i))\Big|_{\phi_1(i), \phi_2(i), f(i), L(i)}$$

$$= \frac{\mu_0 I_{tot}}{4\pi(R_2 - R_1)\phi_{tot}} \sum_{i=1}^{N} \tilde{I}(\rho, \phi, z + \Delta(i))\Big|_{\phi_1(i), \phi_2(i), f(i), L(i)}$$

if the current in each coil is taken to be in the ratio of the azimuthal width of each coil:

$$I(i) = \frac{I_{tot}}{\phi_{tot}} \phi_s(i), \quad \phi_{tot} = \sum_{i=1}^{N} \phi_s(i), \quad I_{tot} = \sum_{i=1}^{N} I(i)$$

The harmonic expansion result (for a current sheet at R) is

$$\vec{B}_{tot,ends}(\rho,\phi,z) = \frac{4\mu_0 I_{tot}}{\pi R^2 \phi_{tot}} \rho_0 \sum_{i=1}^{N} Sin[\phi_s(i)]Cos[2\phi_1(i)+\phi_s(i)] \sum_{k\ odd}\left[\frac{\rho}{\rho_0}\right]^{2k-2} \vec{\vec{V}}_k(\phi) \bullet \sum_{r=0}\left[\frac{\rho}{\rho_0}\right]^{2r} \vec{\vec{\delta}}^{ends}(r,k,\chi+\frac{\Delta(i)}{s(i)})\Big|_{\phi_1(i),\phi_2(i),f(i),s(i)}$$

$$= \frac{4\mu_0 I_{tot}\sigma}{\pi R^2 \phi_{tot}} \rho_0 \sum_{i=1}^{N} \frac{Sin[\phi_s(i)]Cos[2\phi_1(i)+\phi_s(i)]}{\sigma} \sum_{k\ odd}\left[\frac{\rho}{\rho_0}\right]^{2k-2} \vec{\vec{V}}_k(\phi) \bullet \sum_{r=0}\left[\frac{\rho}{\rho_0}\right]^{2r} \vec{\vec{\delta}}^{ends}(r,k,\chi+\frac{\Delta(i)}{s(i)})\Big|_{\phi_1(i),\phi_2(i),f(i),s(i)}$$

$$= G_{tot}\rho_0 \sum_{k\ odd}\left[\frac{\rho}{\rho_0}\right]^{2k-2} \vec{\vec{V}}_k(\phi) \bullet \sum_{r=0}\left[\frac{\rho}{\rho_0}\right]^{2r} \sum_{i=1}^{N} \frac{Sin[\phi_s(i)]Cos[2\phi_1(i)+\phi_s(i)]}{\sigma} \vec{\vec{\delta}}^{ends}(r,k,\chi+\frac{\Delta(i)}{s(i)})\Big|_{\phi_1(i),\phi_2(i),f(i),s(i)}$$

$$\vec{B}_{tot,body}(\rho,\phi,z) = G_{tot}\rho_0 \sum_{k\ odd}\left[\frac{\rho}{\rho_0}\right]^{2k-2} \vec{\vec{V}}_k(\phi) \bullet \sum_{r=0}\left[\frac{\rho}{\rho_0}\right]^{2r} \sum_{i=1}^{N} \frac{Sin[\phi_s(i)]Cos[2\phi_1(i)+\phi_s(i)]}{\sigma} \vec{\vec{\delta}}^{body}(r,k,\chi+\frac{\Delta(i)}{s(i)})\Big|_{\phi_1(i),\phi_2(i),f(i),s(i)}$$

in which

$$\sigma = \sum_{i=1}^{N} Sin[\phi_s(i)]Cos[2\phi_1(i)+\phi_s(i)]$$

$$G_{tot} = \frac{4\mu_0 I_{tot}\sigma}{\pi R^2 \phi_{tot}}$$

The integrated fields are then

$$\vec{B}^{int}_{body}(\rho,\phi) = \int_{-\infty}^{\infty} dz \vec{B}_{body}(\rho,\phi,z) = RG_{tot}\rho_0 \sum_{k\ odd}\left[\frac{\rho}{\rho_0}\right]^{2k-1} \vec{\vec{V}}_k(\phi) \bullet \sum_{r=0}\left[\frac{\rho}{\rho_0}\right]^{2r} \sum_{i=1}^{N} \frac{Sin[\phi_s(i)]Cos[2\phi_1(i)+\phi_s(i)]}{\sigma} \vec{\vec{\delta}}^{body}(r,k)\Big|_{\phi_1(i),\phi_2(i),f(i),s(i)}$$

$$\vec{B}^{int}_{ends}(\rho,\phi) = \int_{-\infty}^{\infty} dz \vec{B}_{end}(\rho,\phi,z) = RG_{tot}\rho_0 \sum_{k\ odd}\left[\frac{\rho}{\rho_0}\right]^{2k-1} \vec{\vec{V}}_k(\phi) \bullet \sum_{r=0}\left[\frac{\rho}{\rho_0}\right]^{2r} \sum_{i=1}^{N} \frac{Sin[\phi_s(i)]Cos[2\phi_1(i)+\phi_s(i)]}{\sigma} (\vec{\vec{\delta}}^{far\ end,tot}(r,k) + \vec{\vec{\delta}}^{near\ end,tot}(r,k))\Big|_{\phi_1(i),\phi_2(i),f(i),s(i)}$$

$$\vec{B}^{int}_{total}(\rho,\phi) = \vec{B}^{int}_{body}(\rho,\phi) + \vec{B}^{int}_{ends}(\rho,\phi)$$

For example, the integrated kth-harmonic becomes

$$L_{eff} b_{2k} = R \sum_{i=1}^{N} \frac{Sin[\phi_s(i)]Cos[2\phi_1(i)+\phi_s(i)]}{\sigma} \left[2\bar{\delta}^{tot,end}_{\rho}(0,k) + \bar{\delta}^{tot,body}_{\rho}(0,k)\right]\Big|_{\phi_1(i),\phi_2(i),f(i),s(i)}$$

$$b_{2k} = \left[\frac{\rho_0}{R}\right]^{2k-2} \frac{1}{s_{eff}\sigma} \sum_{i=1}^{N}\left[s(i)\frac{Sin[2k\phi_2(i)] - Sin[2k\phi_1(i)]}{2k} + 2(-1)^{\frac{k-1}{2}} \bar{I}_i(k)\right]$$

in which

$$\bar{I}_i(k) = \int_0^{\phi_s(i)} d\delta(f(i)\theta_1(i)+\delta) \int_0^{\frac{\pi}{2}} d\alpha Sin[2kh_i(\alpha,\delta)]Sin[\alpha]$$

The integrated longitudinal harmonic (one end only) is

$$\hat{b}_{2k} = \left[\frac{\rho_0}{R}\right]^{2k-1} \frac{1}{s_{eff}\sigma} \sum_{i=1}^{N} \int_0^{\phi_s} d\delta(\theta_1(i)+\delta) \int_0^{\frac{\pi}{2}} d\alpha Cos[2kh_i(\alpha,\delta)]Cos[\alpha]$$

The effective length is

$$L_{eff} = \frac{1}{\sigma}\sum_{i=1}^{N}\left[L(i)\frac{\mathrm{Sin}[2\phi_2(i)] - \mathrm{Sin}[2\phi_1(i)]}{2} + 2R\bar{I}_i(1)\right]$$

If the coils are arranged so that $\phi_1(i+1)=\phi_2(i)$, then

$$\sum_{i=1}^{N}\left[s(i)\frac{\mathrm{Sin}[2k\phi_2(i)] - \mathrm{Sin}[2k\phi_1(i)]}{k}\right] = \frac{s_0}{k}\sum_{i=1}^{N}\left[\mathrm{Sin}[2k\phi_2(i)] - \mathrm{Sin}[2k\phi_1(i)]\right] + \frac{2}{kR}\sum_{i=1}^{N}\Delta(i)\left[\mathrm{Sin}[2k\phi_2(i)] - \mathrm{Sin}[2k\phi_1(i)]\right]$$

$$= \frac{s_0}{k}\left[\mathrm{Sin}[2k\phi_2(N)] - \mathrm{Sin}[2k\phi_1(1)]\right] + \frac{2}{kR}\sum_{i=1}^{N}\Delta(i)\left[\mathrm{Sin}[2k\phi_2(i)] - \mathrm{Sin}[2k\phi_1(i)]\right]$$

So

$$b_{2k} = \left[\frac{\rho_0}{R}\right]^{2k-2}\frac{1}{s_{eff}\sigma}\left[\begin{array}{l}\frac{s_0}{2k}\left[\mathrm{Sin}[2k\phi_2(N)] - \mathrm{Sin}[2k\phi_1(1)]\right] + \\ \sum_{i=1}^{N}\left[\frac{\Delta(i)}{kR}\left[\mathrm{Sin}[2k\phi_2(i)] - \mathrm{Sin}[2k\phi_1(i)]\right] + 2(-1)^{\frac{k-1}{2}}\bar{I}_i(k)\right]\end{array}\right]$$

For $\phi_1(1)=0$, and $\phi_2(N)=\phi_{tot}$ chosen so that $\mathrm{Sin}[2k\phi_2(N)]=0$ for k=3 (1st allowed body harmonic vanishes), then the residual end b_6 harmonic

$$b_6 = \left[\frac{\rho_0}{R}\right]^4\frac{1}{s_{eff}\sigma}\sum_{i=1}^{N}\left[\frac{\Delta(i)}{3R}\left[\mathrm{Sin}[6\phi_2(i)] - \mathrm{Sin}[6\phi_1(i)]\right] - 2\bar{I}_i(3)\right]$$

can be arranged to vanish for a suitable coil arrangement. The first term, which is due to the extension of the straight parts of the coils, can cancel the effect of the second term, which is the contribution from the curved parts of the ends.

The above expression for the effective length is for a flat coil of radius R. For a thick coil which extends from R_1 to R_2, the harmonics and effective length should be calculated by using $R = \frac{R_1 + R_2}{2}$. This will be good to better than a few percent. A better approximation for the effective length can be obtained by multiplying the result above by $\frac{R_1 R_2}{R^2}$.

7. Results for a specific coil geometry

The above expressions for the fields and the harmonics are given as closed analytical results, but involve two-dimensional integrals over the coil end geometry. In obtaining results, these integrals have been done numerically. Two computer programs have been written to evaluate the expressions. One program, written for the program Mathematica, is useful in producing graphs of the harmonics and in debugging the numerical integration algorithms. The other program, written in VAX FORTRAN, is necessary to evaluate the two-dimensional integrals rapidly. The existence of two programs allows each to be checked against the other, reducing the probability of mistakes. Also, the direct method and the harmonic expansion method give expressions for the field which should agree in regions within the coil where both methods are applicable. The coil block results and the current sheet results should agree for very thin coil blocks. Finally, the divergence of the field (computed numerically) should be zero everywhere, and the curl of the field should equal μ_0 times the volume current density. The results of these cross-checks are given in Appendix 5.

(a). "Baseline" coil geometry

After exploring the dependencies of the field and harmonics on the coil end geometry, a "baseline" coil design was established which generally meets the specified requirements for the CESR Q1/Q2 magnets. Specifically, the requirements are (a) lower field in the coil ends than the coil body; if possible; (b) satisfactory integrated harmonic structure for the field ($<5\times10^{-4}$); (c) effective length in the range 630-670 mm; (d) overall physical length of the coils <830 mm. This latter requirement is somewhat soft since it depends on the detailed design of the cold mass and cryostat. Table 1 gives the coil geometry and electrical parameters in the terminology of this note.

Table 1-Baseline Coil Parameters

Current (A)	Number of turns/pole	R_1 (mm)	R_2 (mm)	$R_0=1/2(R_1+R_2)$ (mm)	L_0 (mm)	L_{eff}(mm)
1460	320	97	129	113	460	669

Coil #	Δ(mm)	ϕ_1(rad)	ϕ_2(rad)	ϕ_s(rad)	θ_1(rad)	f	Full length (mm)
1	65	0.0	.415	.415	.370	0.9	783
2	0	0.415	.524	.109	.262	0.9	548.8

The end coil layout is shown in figure 6 (at R=129 mm)

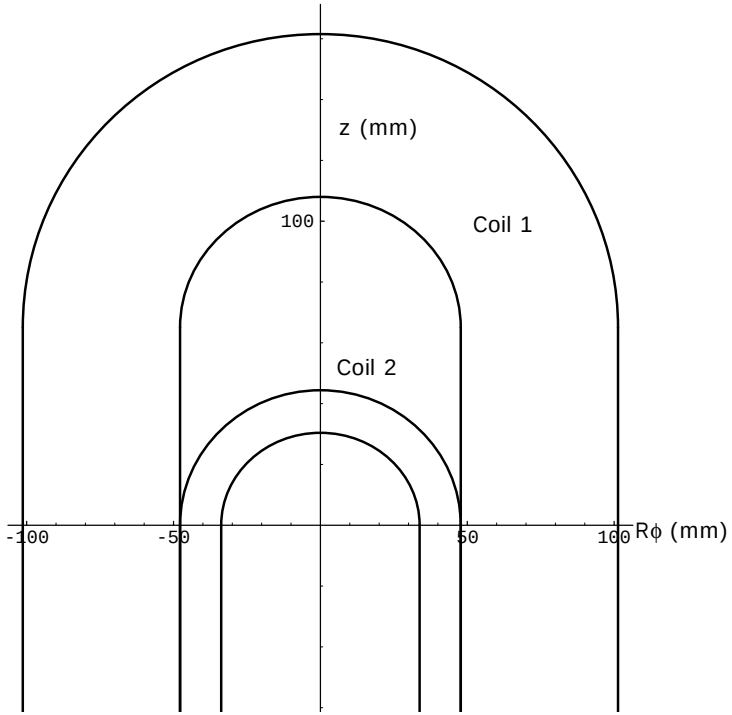

Figure 6
Baseline end coil layout

(b). Integrated harmonics

The integrated "2D" harmonics (b_{2k}) are given in table 2. They are calculated for a current sheet of radius R_0. The effective length for the baseline coil calculates to 668.8 mm. The length of the body plus one end is 621.5 mm.

Harmonic number (k)	1	3	5	7
b_{2k}	10000	-.33	-2.9	0.05
$\hat{b}_{2k}$	374	.0001	-.02	.0004

Table 2: Baseline coil integrated harmonics (in units; 1 unit=10^{-4})

The small value of the b_6 harmonic has been achieved by canceling the contribution from the curved parts of coil 1 and 2 with that due to the straight extension of coil 1 in the end region, as discussed above. The tradeoff between the shape of coil 2 and coil 1 is exhibited in fig. 7, which is a plot of the contours of constant b_6 vs. the coil 1 aspect ratio f(1) and the coil 2 aspect ratio f(2).

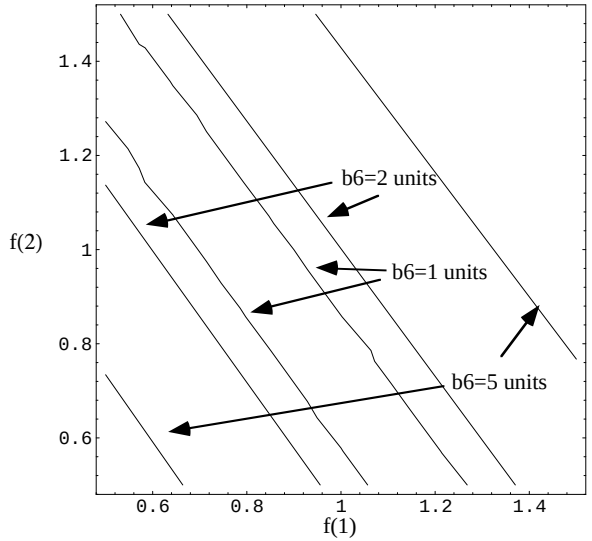

Fig. 7
Contours of constant b_6 vs. f(1) and f(2)
For $\Delta(1)$=65. mm

Fig. 7 shows that one can maintain a small b_6 by simultaneously increasing f(1) and decreasing f(2).

The effect of the large longitudinal harmonic shown in table 2 needs study using beam optics. The longitudinal field only couples through the transverse momentum, so the effective value of the harmonic given above should be multiplied by the transverse angle of the particle relative to the quad axis. For example, if we wish the effective harmonic to be less than 5 units, then table 2 requires that the largest transverse angle be about 5/374=13 mrad (at the reference radius of 5 cm). This ignores the cancellation effects of one end on the other.

(c). Harmonic coefficients

Figures 8 through 19 show the full dependencies of the harmonic coefficients $\delta_{\phi,\rho,z}(r,k,\chi)$on χ. The coefficients up to r=2 (for k=1), k=3, and k=5 are shown. The harmonic coefficients shown in the figures must be scaled by the factors shown ($10^4\eta_0^{(2k-2+2r)}$, where $\eta_0 = 50/R_0$=.4347), to convert to units (10^{-4}). The short dash lines are the contributions from the body; the long-dash lines, from the ends; the solid lines, the total.

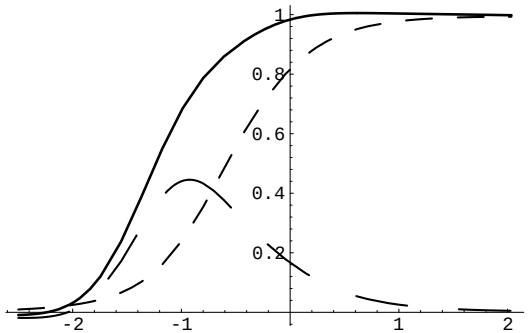

Fig. 8 $\delta_\phi(0,1,\chi)$ vs. χ
Scale factor=10000

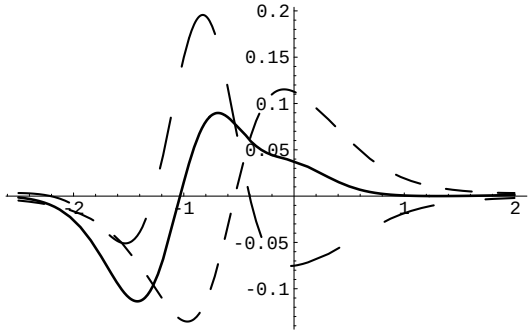

Fig. 9 $\delta_\phi(1,1,\chi)$ vs. χ
Scale factor=1890

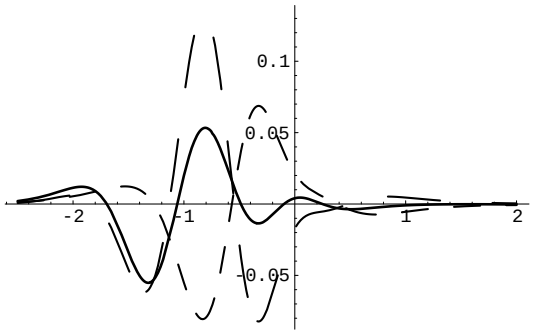

Fig. 10 $\delta_\phi(2,1,\chi)$ vs. χ
Scale factor=357

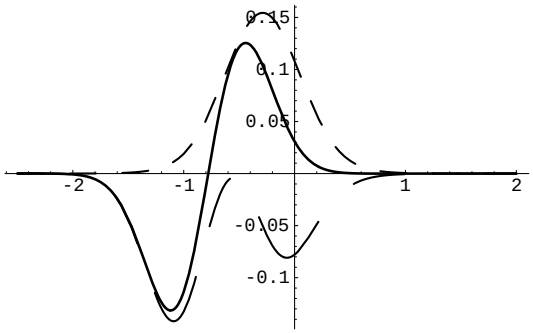

Fig. 11 $\delta_\phi(0,3,\chi)$ vs. χ
Scale factor=357

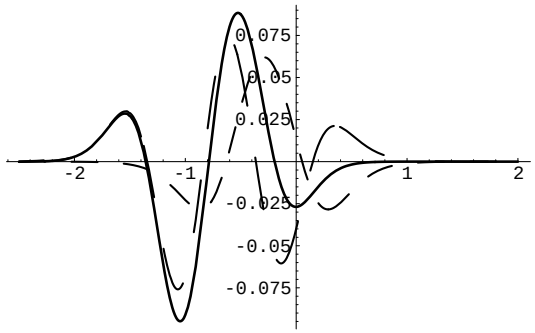

Fig. 12 $\delta_\phi(1,3,\chi)$ vs. χ
Scale factor=67.5

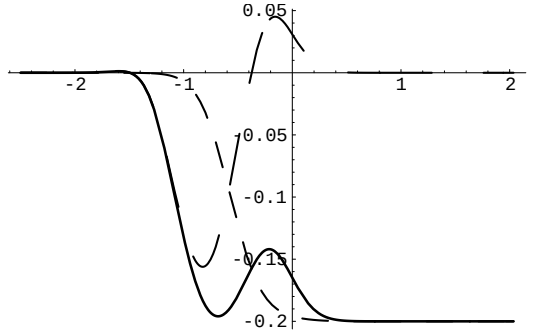

Fig. 13 $\delta_\phi(0,5,\chi)$ vs. χ
Scale factor=12.75

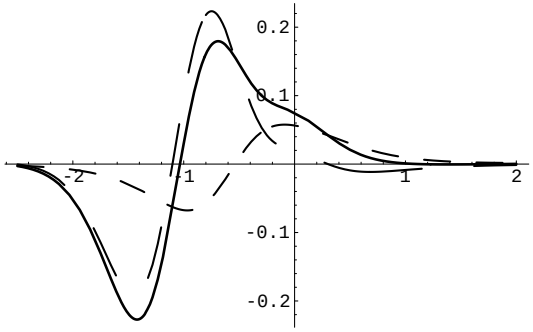

Fig. 14 $\delta_\rho(1,1,\chi)$ vs. χ
Scale factor=1890

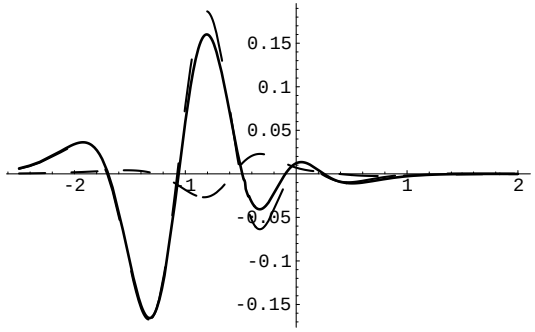

Fig. 15 $\delta_\rho(2,1,\chi)$ vs. χ
Scale factor=357

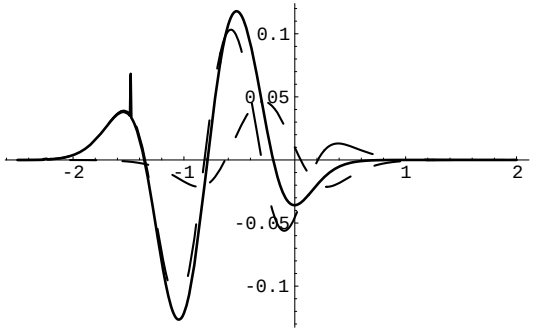

Fig. 16 $\delta_\rho(1,3,\chi)$ vs. χ
Scale factor=67.5

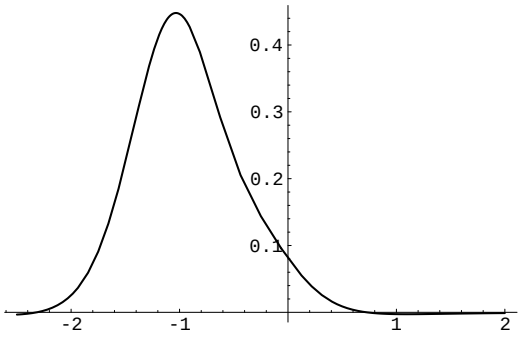

Fig. 17 $\delta_z(1,1,\chi)$ vs. χ
Scale factor=4347

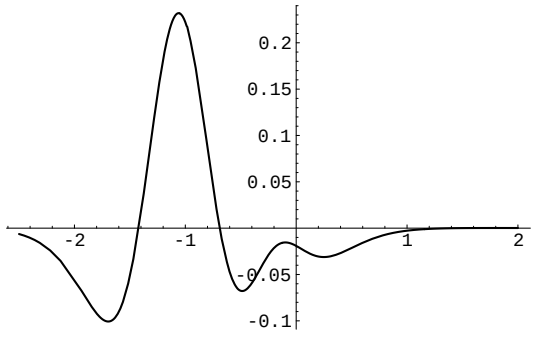

Fig. 18 $\delta_z(2,1,\chi)$ vs. χ
Scale factor=821

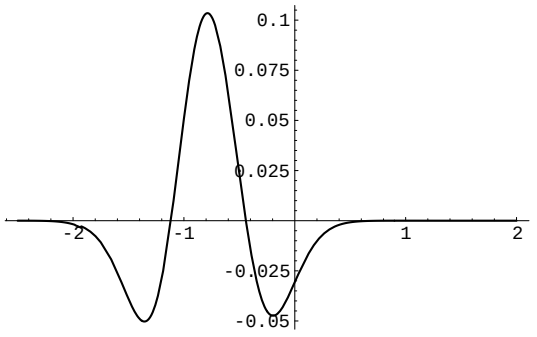

Fig. 19 $\delta_z(1,3,\chi)$ vs. χ
Scale factor=155

(d). Partially integrated harmonics

We can calculate "partial integrals" of the field, which can be used to study the beam optics of the quadrupole field. We define the partial z-integrals

$$\int_{z_1}^{z_2} B_{ends,z}(\rho,\phi,z)dz = RG\rho_0 \sum_{k\ odd} Sin(2k\phi)\left[\frac{\rho}{\rho_0}\right]^{2k-2} \sum_{r=1}\left[\frac{\rho}{\rho_0}\right]^{2r} \int_{\chi_1}^{\chi_2} \delta_z^{ends}(r,k,\chi)d\chi$$

$$= B_0 L_{eff} \sum_{k\ odd} Sin(2k\phi)\left[\frac{\rho}{\rho_0}\right]^{2k-2} \sum_{r=1}\left[\frac{\rho}{\rho_0}\right]^{2r} \tilde{\delta}_z(r,k,\chi_2,\chi_1)$$

$$\int_{z_1}^{z_2} [B_{ends,\phi}(\rho,\phi,z) + B_{body,\phi}(\rho,\phi,z)]dz = G\rho_0 \sum_{k\ odd} Cos(2k\phi)\left[\frac{\rho}{\rho_0}\right]^{2k-1} \sum_{r=0}\left[\frac{\rho}{\rho_0}\right]^{2r} \int_{\chi_1}^{\chi_2} \left[\delta_\phi^{ends}(r,k,\chi) + \delta_\phi^{body}(r,k,\chi)\right]d\chi$$

$$= B_0 L_{eff} \sum_{k\ odd} Sin(2k\phi)\left[\frac{\rho}{\rho_0}\right]^{2k-2} \sum_{r=1}\left[\frac{\rho}{\rho_0}\right]^{2r} \tilde{\delta}_\phi(r,k,\chi_2,\chi_1)$$

$$\int_{z_1}^{z_2} [B_{ends,\rho}(\rho,\phi,z) + B_{body,\rho}(\rho,\phi,z)]dz = G\rho_0 \sum_{k\ odd} Cos(2k\phi)\left[\frac{\rho}{\rho_0}\right]^{2k-1} \sum_{r=0}\left[\frac{\rho}{\rho_0}\right]^{2r} \int_{\chi_1}^{\chi_2} \left[\delta_\rho^{ends}(r,k,\chi) + \delta_\rho^{body}(r,k,\chi)\right]d\chi$$

$$= B_0 L_{eff} \sum_{k\ odd} Sin(2k\phi)\left[\frac{\rho}{\rho_0}\right]^{2k-2} \sum_{r=1}\left[\frac{\rho}{\rho_0}\right]^{2r} \tilde{\delta}_\rho(r,k,\chi_2,\chi_1)$$

in which

$$\tilde{\delta}_z(r,k,\chi_2,\chi_1) = \frac{1}{s_{eff}} \int_{\chi_1}^{\chi_2} \delta_z^{ends}(r,k,\chi)d\chi;\ \tilde{\delta}_\phi(r,k,\chi_2,\chi_1) = \frac{1}{s_{eff}} \int_{\chi_1}^{\chi_2} \left[\delta_\phi^{ends}(r,k,\chi) + \delta_\phi^{body}(r,k,\chi)\right]d\chi;\ \tilde{\delta}_\rho(r,k,\chi_2,\chi_1) = \frac{1}{s_{eff}} \int_{\chi_1}^{\chi_2} \left[\delta_\rho^{ends}(r,k,\chi) + \delta_\rho^{body}(r,k,\chi)\right]d\chi$$

Using the expressions found in Appendix 3(b), we can do the χ integrals analytically. We divide the region from the z=0 end of the magnet to the center of the magnet at $z=L_0/2$, and calculate the field harmonic integrals over segments of this region. The integrated field for each segment is then given by scaling the integrated harmonic with the ρ and ϕ dependence shown above, and multiplying by an overall factor $10^{-4}B_0L_{eff}$ $=10^{-4}G\rho_0L_{eff}$ (= $1.62x10^{-4}$ T-m for the baseline design). Table 3 gives the definition of the regions of $\chi=z/R_0$; the integrated field for each region is effectively located in z at the value of χ_{avg} as given in table 3. The values of the integrated harmonics for each region, and their sum over half the magnet, are shown in table 4.

Region number	χ_1	χ_2	$\chi_{avg}=1/2(\chi_2+\chi_1)$
1	2	2.0354	2.0177
2	1	2	1.5
3	.5	1	.75
4	0.	.5	.25
5	-.5	0	-.25
6	-1	-.5	-.75
7	-1.5	-1	-1.25
8	-2	-1.5	-1.75
9	-3	-2	-2.5

Table 3: definitions of regions of z for partially integrated harmonics

	Region									
Harmonic: (component,k,r)	**1**	**2**	**3**	**4**	**5**	**6**	**7**	**8**	**9**	**Sum**
ϕ**,1,0**	60	1692	849	837	765	560	222	26	-13	4999
ϕ**,1,1**	0	1	3	20	42	61	-62	-56	-8	0
ϕ**,1,2**	0	-1	-2	0	-5	31	-29	0	6	0
ϕ**,3,0**	0	0	0	0	3	0	-3	0	0	0
ϕ**,5,0**	0	-.4	-.2	-.2	-.2	-.2	0	0	0	-1.3
ρ**,1,0**	60	1692	849	837	765	560	222	26	-13	4999
ρ**,1,1**	0	0	7	41	84	121	-125	-112	-16	0
ρ**,1,2**	0	-1	-6	1	-15	92	-87	-1	18	0
ρ**,3,0**	0	0	0	0	3	0	-3	0	0	0
ρ**,5,0**	0	-.4	-.2	-.2	-.2	-.2	0	0	0	-1.3
z,1,1	0	-2	0	14	54	129	135	38	1	370
z,1,2	0	0	-4	-10	-13	21	46	-30	-10	0
z,1,3	0	0	1	-3	1	-6	20	-17	4	0

Table 4: Partially integrated harmonics (units)

(e) Peak field

The coil block model was used to calculate the peak field in the body and ends of the magnet. The peak fields in the ends tend to occur at $\phi=45^o$, at the center of the coil block radially, and at the inner (smallest absolute value) of z for each coil. One can optimize the coil block arrangement by adjusting the azimuthal extent of each of the coil blocks so that the peak fields in each block at the ends are roughly equal. The baseline coil arrangement resulted from such an optimization. The peak fields are given in table 5.

	End peak field, coil 1	**End peak field, coil 2**	**Body peak field, coil 2**
Magnitude	5.49 T	5.53 T	5.73 T
ρ	105.2 mm	103.2 mm	104.8 mm
ϕ	44.2^o	43.5^o	30.0^o
z	-100.07 mm	-24.2 mm	229.4 mm

Table 5: Peak fields in the body and ends

Finally, in table 6 we show the variations in effective length, 12-pole, peak field, and coil length for small changes from the "baseline" (first line of table 6).

f(1)	**f(2)**	ϕ_2**(1)**	Δ**(1) (mm)**	b_6 **(units)**	L_{eff} **(mm)**	**Coil length (mm)**	B_{peak} **(end-coil 2) (T)**	B_{peak} **(end-coil 1) (T)**	B_{peak} **(body) (T)**
.9	.9	.415	65	-.33	669	783	5.53	5.49	5.73
.9	.9	.435	65	-3.2	673	784	5.38	5.71	5.73
.9	.9	.395	65	2.3	664	783	5.66	5.25	5.73
.9	.9	.415	60	-1.7	660	773	5.55	5.48	5.73
.9	.9	.415	70	1.0	677	793	5.51	5.49	5.73
.8	.9	.415	65	0.7	663	773	5.54	5.47	5.73
1.0	.9	.415	65	-1.5	676	794	5.52	5.51	5.73
.9	.8	.415	65	0.4	668	783	5.50	5.49	5.73
.9	1.0	.415	65	-1.1	669	783	5.55	5.49	5.73

Table 6: Variations of the coil geometry about the baseline

8. Conclusion

Expressions have been developed for the three-dimensional magnetic fields of a quadrupole coil, with an end geometry similar to that used in superconducting accelerator magnets. The expressions may be used to calculate either the harmonics of the quadrupole field in the aperture, or the maximum value of the fields within the coils. The approach taken here leads to closed analytical results for the fields, which may be particularly useful in gaining some intuition about the harmonic effects in the ends. In practice, a two-dimensional numerical integration must be performed to obtain results, which, however, may be done relatively rapidly. Numerical calculations using these formulae have been carried out using two computer programs, for the specific case of an example design for the CESR Phase III IR quads. In the example design, good harmonic dependence has been obtained for the integrated fields, and the peak fields in the coil ends have been reduced to less than the peak body field. Estimates of the longitudinal fields in the aperture have been made.

9. Appendices

These are too long to be included here. Copies are available from the author on request.